

# GEOMETRIC MEDIAN SHAPES

Alexandre Cunha

Center for Advanced Methods in Biological Image Analysis  
Center for Data Driven Discovery  
California Institute of Technology, Pasadena, CA, USA

## ABSTRACT

We present an algorithm to compute the geometric median of shapes which is based on the extension of median to high dimensions. The median finding problem is formulated as an optimization over distances and it is solved directly using the watershed method as an optimizer. We show that the geometric median shape faithfully represents the true central tendency of the data, contaminated or not. It is superior to the mean shape which can be negatively affected by the presence of outliers. Our approach can be applied to manifold and non manifold shapes, with single or multiple connected components. The application of distance transform and watershed algorithm, two well established constructs of image processing, lead to an algorithm that can be quickly implemented to generate fast solutions with linear storage requirement. We demonstrate our methods in synthetic and natural shapes and compare median and mean results under increasing outlier contamination.

**Index Terms**— Shape Analysis, Geometric Median, Median Shape, Average Shape, Segmentation Fusion

## 1. INTRODUCTION

The computation of an average shape from a collection of similar shapes is an important tool when classifying, comparing, and searching for objects in a database or in an image. It is helpful, for example, when morphology is key in the identification of healthy and diseased cells, when differentiating wild from mutated cells, in the construction of anatomical atlases, and when combining different candidate segmentations for the same image. The average usually takes the form of the mean or the median, the latter being preferred due to its robustness to automatically filter out outliers. Shape analysis is a vast field of research and many solutions have been proposed to determine geometrical and statistical mean shapes (see *e.g.* [1, 2]), with applications ranging from cell biology to space exploration and methods in the fields of elastic shape analysis [3, 4] and most recently in deep learning for shape analysis [5, 6, 7].

Comparatively, very few have proposed methods for computing medians of shapes. Fletcher *et al.* [8] developed a method to compute the geometric median on Riemannian shape manifolds showing robustness to outliers on the Kendall shape space. In [9] the authors formulate the median finding problem as a variational problem taking into account the area of the symmetric difference of shapes, a model investigated much earlier in [10]. More recently, the work in [11] represents shapes as integral currents and consider median finding using a variational formulation which the authors claim lead to

Funding supporting this work was provided by the Beckman Institute at Caltech, a research center endowed with funds from the Arnold and Mabel Beckman Foundation, to the Center for Advanced Methods in Biological Image Analysis. Correspondence should be addressed to [cunha@caltech.edu](mailto:cunha@caltech.edu).

an efficient linear program in practice. They observed that smooth shapes do not necessarily lead to smooth medians, an aspect we also verified in some of our experiments.

We propose a method to quickly build median shapes from closed planar contours representing silhouettes of shapes discretized in images. Our median shape is computed using the notion of geometric median [12], also known as the spatial median, Fermat-Weber point, and  $L_1$  median (see [13] for the history and survey of multidimensional medians), which is an extension of the median of numbers to points in higher dimensional spaces. The geometric median has the property, in any dimension, that it minimizes the sum of its Euclidean distances to given anchor points  $x_j \in \mathbb{R}^n$ ,

$$x^* = \arg \min_x \sum_j \|x - x_j\| \quad . \quad (1)$$

It has a breakdown point of 0.5, *i.e.* the data can be corrupted with up to 50% and it still gives a good prediction representing the sample [14] (and [15] for the functional median). Unlike the mean (centroid) of points, which can be found directly using an analytical expression, the geometric median can only be approximated by numerical algorithms. Due to convexity of eq.(1) the median point always exist and it is unique provided the anchor points are not collinear [16]. The geometric median lies within the convex hull of the given points (see *e.g.* [17]), a property we will exploit in our approach.

Researchers have developed fast numerical solutions for this convex problem. Weiszfeld developed in 1937, at the age of 16 years old, a gradient descent algorithm which is still quite competitive (see translated reprint [18], and [19] for a review). It was rediscovered many times until recognition on early 60's. New developments claim faster algorithms that can handle large data sets [20, 21]. We do not rely on these methods as our median shape is generated by finding paths of minimum cost in the discrete image domain.

The emphasis of our presentation is to introduce a novel algorithm capable of generating median shapes in a fast manner using tools already familiar to the image processing community. We will leave proofs for the mathematical models and formulations presented here for future work.

## 2. METHODS

### 2.1. A distance for planar shapes

We define here the expression to measure the distance between closed planar shapes represented by their contours. It is this metric that we will be optimizing when computing the geometric median of a set of shapes. We assume contours are rectifiable curves, but do not restrict their topology to planar manifolds, crossings are allowed. Other popular metrics to measure distances between shapes,

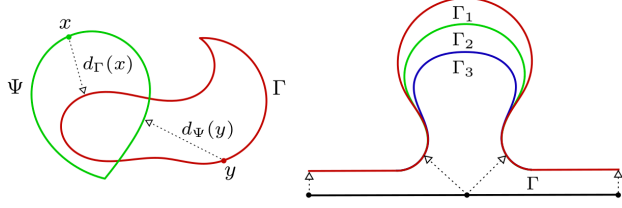


**Fig. 1: Illustration of planar shape distances.** Arrows in the left figure represent the shortest distances  $d_\Gamma(x)$  and  $d_\Psi(y)$  from points  $x \in \Psi$  and  $y \in \Gamma$ , respectively, to closed contours  $\Gamma$  and  $\Psi$ . The figure on the right illustrates a case where the horizontal black curve  $\Gamma$  is equally distant to three different other curves,  $d(\Gamma, \Gamma_1) = d(\Gamma, \Gamma_2) = d(\Gamma, \Gamma_3) = 63$ . The symmetric distance  $d_g$  captures our two-way expectations:  $d_g(\Gamma, \Gamma_1) = 145 > d_g(\Gamma, \Gamma_2) = 129 > d_g(\Gamma, \Gamma_3) = 116$ . Curves  $\Gamma_i$  only differ at the bulgy part. Slanted arrows on the right figure are directed to the farthest points on  $\Gamma_i$  from  $\Gamma$ . To compute  $d_g$ , curves were 8-connected discretized in 429x295 images.

e.g. Hausdorff and Fréchet distances, are not suitable for our median formulation as they do not report distances along the entire length of candidate curves.

Let  $d_\Gamma: \mathbb{R}^2 \rightarrow \mathbb{R}$  give the distance of a point  $x \in \mathbb{R}^2$  to a curve  $\Gamma \subset \mathbb{R}^2$ ,

$$d_\Gamma(x) = \inf_{y \in \Gamma} \|x - y\| \geq 0 \quad (2)$$

where the infimum is attained for one or more points  $y \in \Gamma$  closest to  $x$ , and the  $L_2$  norm  $\|\cdot\|$  gives the Euclidean distance between points (see Fig.1). Note that  $d_\Gamma(x) = 0 \Leftrightarrow x \in \Gamma$ . We then define the distance from a rectifiable curve  $\Gamma$  to another curve  $\Psi$  using a line integral over all points  $x := x(s) \in \Gamma$ ,

$$d(\Gamma, \Psi) = \frac{1}{|\Gamma|} \int_\Gamma d_\Psi(x) ds \quad (3)$$

where  $d_\Psi(\cdot)$  is given by eq(2),  $ds$  is the arc length differential, and  $|\Gamma| > 0$  is the length of curve  $\Gamma$ . By integrating distances for all points along the curve and dividing by its length we have a measure that tells us how far, in average, is the source curve  $\Gamma$  to the target curve  $\Psi$ . This measure is independent of curve parameterization. It follows that  $d(\Gamma, \Psi) \geq 0$  and  $d(\Gamma, \Psi) = 0 \Leftrightarrow \Gamma = \Psi$ . If  $\Gamma$  and  $\Psi$  are parallel curves for which  $\forall x \in \Gamma, d_\Psi(x) = \delta$ , then  $d(\Gamma, \Psi) = \delta$ , which is what we intuitively expect. As an example, for two concentric circles with radii  $r_1 > r_2$ , we have  $\delta = r_1 - r_2$ . Another property of  $d(\cdot, \cdot)$  is its invariance under isometries (rigid transformations including reflections), owing to the intrinsic property of curve length and to the preservation of point distances under such transformations.

In general, this distance is asymmetric,  $d(\Gamma, \Psi) \neq d(\Psi, \Gamma)$ , unless the curves themselves are symmetric with respect to an axis. Similar to the Hausdorff distance, we combine  $d(\Gamma, \Psi)$  and  $d(\Psi, \Gamma)$  to obtain a symmetric distance  $d_g$ ,

$$d_g(\Gamma, \Psi) = \frac{1}{2} (d(\Gamma, \Psi) + d(\Psi, \Gamma)) \quad (4)$$

possessing the following properties: (1)  $d_g(\Gamma, \Psi) \geq 0$  (non-negativity); (2)  $d_g(\Gamma, \Psi) = 0 \Leftrightarrow \Gamma = \Psi$  (identity); (3)  $d_g(\Gamma, \Psi) = d_g(\Psi, \Gamma)$  (symmetry); (4)  $d_g(\Gamma, \Psi) \leq d_g(\Gamma, \Phi) + d_g(\Phi, \Psi)$ ,  $\forall \Gamma, \Psi, \Phi$  (triangle inequality). Properties (1) to (3) are due to the Euclidean norm used in  $d(\cdot, \cdot)$ . The triangle inequality property requires formal proof, a task for future work. All properties have been experimentally validated.

## 2.2. Geometric median for shapes

We formulate the problem of finding the geometric median of shapes as an optimization problem over distances, similar to the high dimensional geometric median of points: find the optimal closed contour  $\Gamma^*$  that minimizes the sum of distances to a given set of closed contours  $\{\Gamma_i\}_{i=1}^n$ ,

$$\Gamma^* = \arg \min_\Gamma \sum_{i=1}^n d(\Gamma, \Gamma_i) \quad (5)$$

where  $d(\cdot, \cdot)$  is given by eq.(3) and the solution lies in the convex hull of  $\{\Gamma_i\}$ ,  $\Gamma^* \subset ch(\{\Gamma_i\})$ . When each curve  $\Gamma_i$  degenerates to a point, with  $|\Gamma_i| = 1$ , then the problem is reduced to finding the geometric median of points. From eq.(5) we then have

$$\begin{aligned} \Gamma^* &= \arg \min_\Gamma \sum_{i=1}^n \left( \frac{1}{|\Gamma|} \int_\Gamma d_{\Gamma_i}(x) ds \right), \quad x \in \Gamma \\ &= \arg \min_\Gamma \frac{1}{|\Gamma|} \int_\Gamma \left( \sum_{i=1}^n d_{\Gamma_i}(x) \right) ds \\ &= \arg \min_\Gamma \frac{1}{|\Gamma|} \int_\Gamma \left( \sum_{i=1}^n \|x - y_i\| \right) ds, \quad y_i \in \Gamma_i \end{aligned} \quad (6)$$

where  $\int$  and  $\sum$  commute due to Tonelli's theorem for non-negative functions [22] (indeed,  $d_{\Gamma_i}(\cdot) \geq 0$ ) and  $y_i$  is the point in  $\Gamma_i$  closest to  $x \in \Gamma$ , as in Fig.1. It should be clear that the location of each  $y_i$  depends on the position of  $x$  in  $\Gamma$ , thus  $y := y_i(x)$ .

Let's for a moment ignore  $|\Gamma|$  on eq.(6) and consider an approximation of the unknown  $\Gamma$  by an ordered set of points  $(x_1, \dots, x_m)$ . At the solution  $\Gamma^* := (x_1^*, \dots, x_m^*)$ , the term in parentheses on the last expression in eq.(6) is optimized for each  $x_j$  which implies that any point in  $\Gamma^*$  is in fact the geometric median of points  $\{y_i\}_{i=1}^n$ , each from a single  $\Gamma_i$ ,

$$x^* = \arg \min_x \sum_{i=1}^n \|x - y_i\|, \quad y_i \in \Gamma_i, \forall x^* \in \Gamma^* \quad (7)$$

Since we know  $x^* \in ch(\{y_i\}) \subset ch(\{\Gamma_i\})$ , see e.g. [17], we can then show by contradiction that  $\Gamma^* \subset ch(\{\Gamma_i\})$ , as stated above. This is a property that will help us in the optimization. Directly computing each  $x^*$  from points  $y_i(x)$  is not straightforward due to the nonlinear dependency of  $y_i$  on  $x$ . It is also not clear how to properly select a set of  $n$  points  $\{y_i\}$ , one for each curve  $\Gamma_i$ , to produce each median point  $x_j^*$  in  $\Gamma^*$ .

By discarding the contribution of the curve length  $|\Gamma|$  and optimizing solely based on distances, i.e. minimizing the following functional

$$J(\Gamma) = \int_\Gamma \left( \sum_{i=1}^n \|x - y_i(x)\| \right) ds, \quad x \in \Gamma \quad (8)$$

we end up with a simpler problem while, surprisingly, still solving the original optimization problem in eq.(5). Our results consistently demonstrate we are also optimizing for the curve length even though we are not explicitly considering it in the optimization.

When we use a squared norm in eq.(8) and elsewhere, i.e. squared distances  $\|x - y_i\|^2$  instead of  $\|x - y_i\|$ , then we call  $\Gamma^*$  the optimal mean shape. We compare mean and median shapes in our experiments and show the latter is much less sensitive to outliers.

## 2.3. Optimization with watershed transform

We look for the closed contour having overall the smallest sum of distances from its points to all given contours  $\Gamma_i$ . We solve this

problem as an optimal path finding problem where the watershed with markers method [23] is applied over the accumulated distance transforms image of the given curves to generate the median contour  $\Gamma^*$ . Briefly, the basic idea to form the median is as follows. For every grid point  $x$  in the image domain we find its total distance  $\phi(x)$  to all the contours  $\Gamma_i$  – this is what the accumulated distance transform does. The next step is to find those grid points forming a closed path which together have the least sum of total distances,  $\phi(\Gamma^*) < \phi(\Gamma), \forall \Gamma \neq \Gamma^*$ . This is accomplished by the watershed method which computes the closed path with minimum cost.

Others have applied the watershed method to solve optimization problems on either a graph or a discrete grid. For example, Cuprie *et al.* [24] used the Power Watershed [25] in their formulation of the surface reconstruction from point cloud problem to minimize a weighted total variation functional where weights are proportional to Euclidean distances between points.

We abuse the notation here and use  $\Gamma_i$  to designate both the 8-connected contour and the image containing it. We represent each contour  $\Gamma_i$  as the zero level set of a unsigned distance transform function  $\phi_i: \Omega \rightarrow \mathbb{R}_+$ , such that  $\phi_i(x) = 0$  for  $x \in \Gamma_i$ ,  $\phi_i(x) > 0$  for  $x \in \Omega \setminus \Gamma_i$ , and  $\phi_i(x)$  gives the shortest distance from  $x$  to curve  $\Gamma_i$ . Thus, from eq.(2),  $\phi_i(x) = d_{\Gamma_i}(x)$ . If we take the sum  $\phi(x) = \sum_{i=1}^n \phi_i(x)$  for every point  $x$  in the domain  $\Omega$  of the image, the median contour  $\Gamma^*$  is a minimal path in the image  $\phi$ .

To create markers for the watershed, we take the union of the basins in  $\hat{\phi}$  (the inverted  $\phi$ ) with the complement of the convex hull of contours  $\Gamma_i$ ,  $\Omega \setminus ch(\{\Gamma_i\})$ . The marker imposed outside the convex hull prevents the creation of false positive regions due to eventual basins placed close to the boundary of the image. Points in regional minima are those farthest from the contours, and hence serve well as markers. The watershed lines computed from these markers form  $\Gamma^*$ , as presented in the GEMS algorithm below.

---

### GEMS – Geometric Median Shapes

---

```

1: procedure GEMS( $h, \Gamma_1, \dots, \Gamma_n$ )
2:   Input:  $h$  (minima height),  $\Gamma_i$  (contour images)
3:   Output:  $\Gamma^*$  (geometric median)
4:    $\phi = 0$ 
5:   for  $i = 1, \dots, n$  do
6:      $\phi' = \text{EuclideanDistanceTransform}(\Gamma_i)$ 
7:      $\phi = \phi + \phi'$ 
8:   end
9:    $\hat{\phi} = \text{invert}(\phi)$ 
10:   $B = \text{WatershedBasins}(\hat{\phi}, h)$ 
11:   $H = \text{ConvexHull}(\Gamma_1, \dots, \Gamma_n)$ 
12:   $markers = B \cup \{\Omega \setminus H\}$ 
13:   $\Gamma^* = \text{Watershed}(\hat{\phi}, markers)$ 

```

---

Our current implementation of GEMS is a script that uses distance transforms, height minima, minima, convex hull, and watershed implementations from the `pink` [26] and `gmic` [27] packages, with image I/O operations primarily supported by `gmic`. Note that memory space is linear in image size and does not grow with the number of contours  $\Gamma_i$ . The only parameter that needs adjustments is the height  $h$  used for the detection of watershed basins. The `for` loop can be parallelized to speed up computations.

---

When the contours  $\Gamma_i$  are highly dissimilar in shape and location then a shape representing the central tendency of the data is either too weak or non-existent. This is reflected in the value of the height parameter  $h$ : the smaller the  $h$  value needed to create  $\Gamma^*$ , the less cohesive is the data – provided colocalized shapes are not too slim. For example, we could not obtain a median for the colored outliers

in Fig.4, even after taking  $h = 1$ , as they are very dissimilar to each other and dispersed.

When contours reach the boundaries of the image, GEMS results need to be augmented. This is, for example, the case when building a consensus out of many binary contour segmentations  $\{\Gamma_i\}$  for tiles of an image – see Fig.5. Disconnected basins are formed at the boundary of the image  $\hat{\phi}$  and we no longer have the larger marker outside the convex hull to eliminate them. This in turn leads to the creation of extra regions not representing the actual data. We repair this over segmentation, whenever present, by removing edges from  $\Gamma^*$  according to the following criteria: (1) Let  $\Gamma_{or} = \bigcup_i \Gamma_i$ . Edges in  $\Gamma^*$  not present in  $\Gamma_{or}$  are removed: if the edge has no candidate from the pool of segmentations, there is no justification to keep it; this eliminates the great majority of extraneous edges in  $\Gamma^*$ . (2) Edges in  $\Gamma^*$  which have a small count (currently 20%) in the pool  $\{\Gamma_i\}$  and an average intensity close to background are eliminated; this is done to remove edges introduced only by a few users that can be potentially annotation mistakes.

Our experiments have consistently demonstrated that the median shapes  $\Gamma^*$  obtained using GEMS have a cost  $\sum_i d(\Gamma, \Gamma_i)$  lower than any other contour in its vicinity,  $\Gamma = \Gamma^* + \epsilon\Psi, \epsilon \ll 1$ , and elsewhere. One might argue that the cost could be reduced, according to eq.(3), by picking a longer curve. But this is not the case. Choosing a contour  $\Gamma$  longer than  $\Gamma^*$ , a few pixels away from the optimal configuration, increases the sum of distances  $\phi$  at a greater rate, as the accumulated point distances  $\phi(\Gamma)$  grows faster than the curve length  $|\Gamma|$ . Conversely, choosing a curve with fewer points to decrease  $\phi(\Gamma)$  does not reduce the cost  $J(\Gamma)$  as now the curve length is smaller and although we have now fewer points each has a higher accumulated distance. Evidences suggest then that GEMS not only finds the contour with lowest accumulated  $L_1$  distances,  $J(\Gamma)$ , but it also picks the path with the right length. This indicates that  $\Gamma^*$  optimizes distances  $d(\cdot, \cdot)$ , and consequently  $d_g(\cdot, \cdot)$ . We report values for  $d_g$  in our experiments.

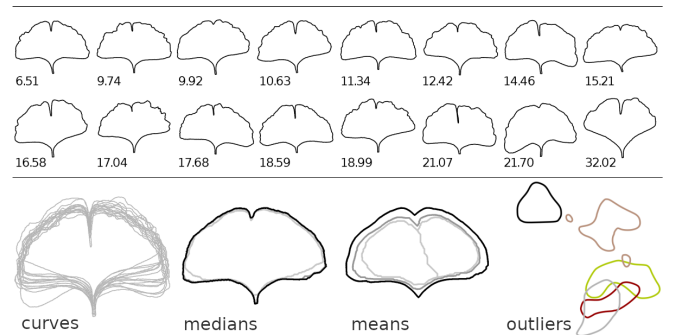


**Fig. 2: Median and mean shapes for *Ginkgo biloba* leaves.** Sixteen leaf curves are ordered according to their  $d_g$  distances to their geometric median. They were midvein aligned and scaled keeping their original aspect ratio and shape, all shown on the `curves` panel. Their respective geometric median and mean shapes are the black curves on the `medians` and `means` panels. Median and mean are 2.63 pixel units  $d_g$  distant. Note that the *petiole* (lower tip) is better captured by the median. The gray median shapes were obtained after tainting data with two (black and brown curves) and five outliers, shown on the rightmost `outliers` panel, resulting in poor average shapes distant 24.11 and 56.75 from the true mean. We can no longer obtain a simple mean curve when these five outliers are considered. These outliers barely affect the median. The gray median, shown on the `medians` panel, is only 10.38 pixel units apart from the true median. It was obtained after contaminating data with ten outliers, twice as much used for the mean, thus illustrating the superiority of the geometric median. Leaf images have 800x800 pixels.

### 3. EXPERIMENTAL RESULTS

We demonstrate GEMS on a set of planar shapes ranging from plant leaves to hand traced circles and non-manifold shapes resulting from interactive segmentation of biological cells. The examples in the figures are self contained and address particular cases of interest. Leaf data is from [28].

In the *Ginkgo biloba* leaves experiment, Fig.2, we compute median and mean shapes for sixteen aligned contours, with and without outliers. Median and mean are initially pretty close,  $d_g = 2.63$ , but their distances increase with the introduction of outliers. The influence of data alignment for the median computation is presented in Fig.3, where tulip leaves are registered in different ways leading to distinct but close in shape medians. We illustrate in the central example, Fig.4, a case that the geometric median holds the central tendency even when the contamination with outliers is beyond 50%. This is not the case for the mean shape which deteriorates quickly as we increase the number of random outliers tainting the data. In the last experiment, Fig.5, we use the augmented GEMS described in section 2.3, to create a consensus segmentation for a small set of interactively generated segmentation results. These segmentations are for small tiles cropped from large cell images. We compare our results with those created by the Staple method [29] and show that our approach is comparable, and sometimes better, and can produce results much faster.

### 4. CONCLUSIONS

We presented an algorithm, GEMS, to compute geometric median shapes which is simple, fast, straightforward to implement and requires adjustments of a single parameter. The approach leads to median shapes that are robust to outliers supporting a contamination of over 50% while still capturing the central tendency of given shapes. We adopted the watershed transform as the optimizer to identify paths of minimal cost in the accumulated distance transform image. Our experiments have shown that the proposed symmetric distance  $d_g$  is optimized for the geometric median contour even though the curve length is not explicitly considered in the optimization. From our initial experimentation, our approach compares well with the Staple method in the segmentation consensus problem while being faster by many orders of magnitude.

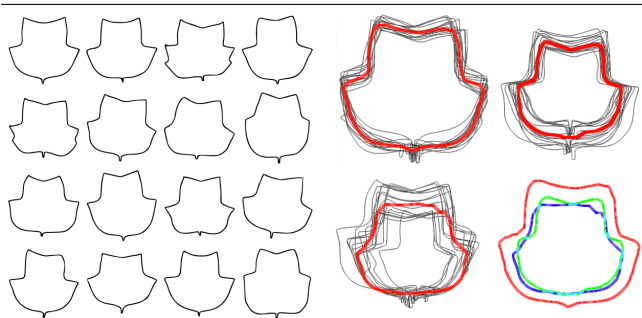


**Fig. 3: Alignment and medians.** Sixteen tulip tree (*Liriodendron tulipifera*) leaves, shown on the left panel, are aligned in different ways leading to different median shapes (bottom right curves) conforming to the alignment. We overlay the medians, shown as thick red contours, onto the aligned leaf curves to visually demonstrate their placement: in the convex hull of the given shapes and not biased towards the extremes – see e.g. the top right case. Registrations were: no registration (top, left), registration to a line passing through side lobe corners (top right), and rigid registration, all done using the same chosen target image from the pool.

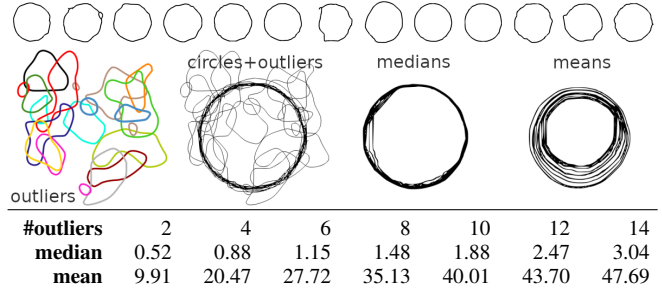


**Fig. 4: Robustness to outliers.** Thirteen noisy circles hand traced by different users, shown on top row, were collected using our *Collaborative Segmentation* web application. We progressively added randomly generated outliers to contaminate the circle data with up to fourteen outliers, 50%+1 contamination (colored rubber bands on outliers panel, one color per outlier, some disconnected). These are strong outliers as they greatly differ in size, shape, topology, and location when compared to the circles – see circles+outliers panel. For each additional outlier added to the pool of circles, we compute new median and mean shapes and then measure their distance  $d_g$  to, respectively, the median and mean shapes obtained without outliers. These numbers are shown on the table above for seven out of fourteen contaminations. The geometric median is marginally affected –  $d_g$  is at most 3 pixel units – while the mean significantly deteriorates, early and quickly. Panels medians and means show respectively geometric median and mean shapes as outliers progress, from one to fourteen. All processed images have 400x400 pixels.

As part of future work, we intend to extend the model and experiments to 3D. We also plan to investigate using distances other than the Euclidean distance which might lead to other types of average shapes. We also plan to adopt weights to combine shapes, in a weighted average fashion, as this might be useful in shape clustering problems. We intend to investigate if and how the distance  $d_g$  and our median shapes can improve classification in large data sets. We are also interested in continuing studying the potential of medians for the segmentation consensus problem in both 2D and 3D, as the need to combine individual segmentations while automatically discarding outliers is of importance to real time collaborative segmentation systems.

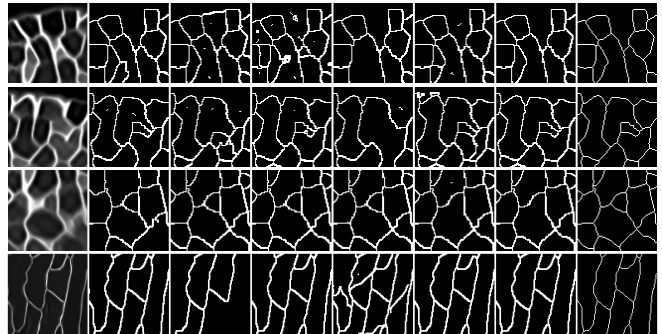


**Fig. 5: Segmentation consensus.** Results of interactive segmentation (columns 2 to 6) are shown for four small tiles (column 1) of much larger images. Although users create different segmentations for the same image, they nevertheless exhibit some agreement most prominent in clear, unambiguous parts of the image. Using our median approach to combine users' segmentations into a single one eliminates outliers and spurious annotations, e.g. dangling scribbles and speckles, as shown in our results on the last column, 8. Our solution is on par or better (third row) than results obtained with the Staple method [29], shown on column 7, and orders of magnitude faster (e.g. 1.06s against 237.35s for sixteen 800x800 images) when compared to the expectation maximization approach adopted by Staple. Users' segmentations are from our *Collaborative Segmentation* web application.  $h = 5$  or 10.

## 5. REFERENCES

- [1] Eric Klassen, Anuj Srivastava, M Mio, and Shantanu H Joshi, “Analysis of planar shapes using geodesic paths on shape spaces,” *IEEE Transactions on Pattern Analysis and Machine Intelligence*, vol. 26, no. 3, pp. 372–383, 2004.
- [2] Luciano da Fona Costa and Roberto Marcond Cesar Jr, *Shape classification and analysis: theory and practice*, CRC Press, 2018.
- [3] Washington Mio, Anuj Srivastava, and Shantanu Joshi, “On shape of plane elastic curves,” *International Journal of Computer Vision*, vol. 73, no. 3, pp. 307–324, 2007.
- [4] Anuj Srivastava, Eric Klassen, Shantanu H Joshi, and Ian H Jermyn, “Shape analysis of elastic curves in Euclidean spaces,” *IEEE Transactions on Pattern Analysis and Machine Intelligence*, vol. 33, no. 7, pp. 1415–1428, 2011.
- [5] Davide Boscaini, Jonathan Masci, Emanuele Rodolà, and Michael Bronstein, “Learning shape correspondence with anisotropic convolutional neural networks,” in *Advances in Neural Information Processing Systems*, 2016, pp. 3189–3197.
- [6] Matthias Vestner, Zorah Löhner, Amit Boyarski, Or Litany, Ron Slossberg, Tal Remez, Emanuele Rodola, Alex Bronstein, Michael Bronstein, and Ron Kimmel, “Efficient deformable shape correspondence via kernel matching,” in *3D Vision (3DV), 2017 International Conference on*. IEEE, 2017, pp. 517–526.
- [7] Thibault Groueix, Matthew Fisher, Vladimir G Kim, Bryan C Russell, and Mathieu Aubry, “3D-CODED: 3D correspondences by deep deformation,” in *Proceedings of the European Conference on Computer Vision (ECCV)*, 2018, pp. 230–246.
- [8] P Thomas Fletcher, Suresh Venkatasubramanian, and Sarang Joshi, “Robust statistics on Riemannian manifolds via the geometric median,” in *Computer Vision and Pattern Recognition, 2008. CVPR 2008*. IEEE, 2008, pp. 1–8.
- [9] Benjamin Berkels, Gina Linkmann, and Martin Rumpf, “An SL (2) invariant shape median,” *Journal of Mathematical Imaging and Vision*, vol. 37, no. 2, pp. 85–97, 2010.
- [10] Alexandre Cunha, *A fully eulerian method for shape optimization, with application to Navier-Stokes flows*, chapter 2: Shape Matching, pp. 9–43, PhD thesis, Carnegie Mellon University, September 2004.
- [11] Yunfeng Hu, Matthew Hudelson, Bala Krishnamoorthy, Altansuren Tumurbaatar, and Kevin R Vixie, “Median shapes,” *arXiv preprint arXiv:1802.04968*, 2018.
- [12] JBS Haldane, “Note on the median of a multivariate distribution,” *Biometrika*, vol. 35, no. 3-4, pp. 414–417, 1948.
- [13] Christopher G Small, “A survey of multidimensional medians,” *International Statistical Review/Revue Internationale de Statistique*, pp. 263–277, 1990.
- [14] Hendrik P Lopuhaä and Peter J Rousseeuw, “Breakdown points of affine equivariant estimators of multivariate location and covariance matrices,” *The Annals of Statistics*, vol. 19, no. 1, pp. 229–248, 1991.
- [15] Daniel Gervini, “Robust functional estimation using the median and spherical principal components,” *Biometrika*, vol. 95, no. 3, pp. 587–600, 2008.
- [16] J. H. B. Kemperman, “The median of a finite measure on a Banach space,” *Statistical Data Analysis Based on the  $L_1$ -norm and Related Methods (Neuchâtel, 1987)*, pp. 217–230, 1987.
- [17] Stanislav Minsker, “Geometric median and robust estimation in Banach spaces,” *Bernoulli*, vol. 21, no. 4, pp. 2308–2335, 2015.
- [18] Endre Weiszfeld and Frank Plastria, “On the point for which the sum of the distances to  $n$  given points is minimum,” *Annals of Operations Research*, vol. 167, no. 1, pp. 7–41, 2009.
- [19] Amir Beck and Shoham Sabach, “Weiszfeld’s method: old and new results,” *Journal of Optimization Theory and Applications*, vol. 164, no. 1, pp. 1–40, 2015.
- [20] Yehuda Vardi and Cun-Hui Zhang, “The multivariate  $L_1$ -median and associated data depth,” *Proceedings of the National Academy of Sciences*, vol. 97, no. 4, pp. 1423–1426, 2000.
- [21] Hervé Cardot, Peggy Cénac, and Pierre-André Zitt, “Efficient and fast estimation of the geometric median in Hilbert spaces with an averaged stochastic gradient algorithm,” *Bernoulli*, vol. 19, no. 1, pp. 18–43, 2013.
- [22] Gerald B Folland, *Real analysis: modern techniques and their applications*, John Wiley & Sons, 2013.
- [23] Serge Beucher and Fernand Meyer, “The morphological approach to segmentation: the watershed transformation,” *Optical Engineering-New York-Marcel Dekker Incorporated-*, vol. 34, pp. 433–433, 1992.
- [24] Camille Couprie, Xavier Bresson, Laurent Najman, Hugues Talbot, and Leo Grady, “Surface reconstruction using power watershed,” in *International Symposium on Mathematical Morphology and Its Applications to Signal and Image Processing*. Springer, 2011, pp. 381–392.
- [25] Camille Couprie, Leo Grady, Laurent Najman, and Hugues Talbot, “Power watershed: a unifying graph-based optimization framework,” *IEEE Transactions on Pattern Analysis and Machine Intelligence*, vol. 33, no. 7, pp. 1384–1399, 2011.
- [26] Michel Couprie, Laszlo Marak, and Hugues Talbot, “The Pink Image Processing Library,” <https://perso.esiee.fr/~coupriem/Pink/doc/html/>.
- [27] David Tschumperlé, “G’MIC, GREYC’s Magic for Image Computing,” <https://gmlic.eu>.
- [28] Charles Mallah, James Cope, and James Orwell, “Plant leaf classification using probabilistic integration of shape, texture and margin features,” *Signal Processing, Pattern Recognition and Applications*, vol. 5, no. 1, 2013.
- [29] Simon K Warfield, Kelly H Zou, and William M Wells, “Simultaneous truth and performance level estimation (STAPLE): an algorithm for the validation of image segmentation,” *IEEE Transactions on Medical Imaging*, vol. 23, no. 7, pp. 903–921, 2004.